OPEN ACCESS

Original research

PARP-1 selectively impairs *KRAS*-driven phenotypic and molecular features in intrahepatic cholangiocarcinoma

Friederike L Keggenhoff,[1] Darko Castven,[2] Diana Becker,[1] Stojan Stojkovic,[2] Jovana Castven,[2] Carolin Zimpel,[2] Beate K Straub,[3,4] Tiemo Gerber,[3] Harald Langer,[5] Patricia Hähnel,[6] Thomas Kindler,[6] Jörg Fahrer,[7] Colm J O'Rourke,[8] Ursula Ehmer,[9] Anna Saborowski,[10] Lichun Ma,[11] Xin Wei Wang,[11,12] Timo Gaiser ,[13] Matthias S Matter,[14] Christian Sina,[15] Stefanie Derer ,[15] Ju-Seog Lee ,[16] Stephanie Roessler ,[17] Bernd Kaina,[18] Jesper B Andersen ,[8] Peter R Galle,[1] Jens U Marquardt [2]

► Additional supplemental material is published online only. To view, please visit the journal online (https://doi.org/10.1136/gutjnl-2023-331237).

For numbered affiliations see end of article.

Correspondence to
Professor Jens U Marquardt, Department of Medicine I, University Medical Center Schleswig Holstein Lübeck Campus, Lubeck, Schleswig-Holstein, Germany; Jens.Marquardt@uksh.de

FLK and DC contributed equally.

Received 19 October 2023
Accepted 24 May 2024

To cite: Keggenhoff FL, Castven D, Becker D, *et al*. *Gut* Epub ahead of print: [*please include* Day Month Year]. doi:10.1136/gutjnl-2023-331237

ABSTRACT

Objective Intrahepatic cholangiocarcinoma (iCCA) is the second most common primary liver cancer with limited therapeutic options. *KRAS* mutations are among the most abundant genetic alterations in iCCA associated with poor clinical outcome and treatment response. Recent findings indicate that Poly(ADP-ribose) polymerase1 (PARP-1) is implicated in *KRAS*-driven cancers, but its exact role in cholangiocarcinogenesis remains undefined.

Design *PARP-1* inhibition was performed in patient-derived and established iCCA cells using RNAi, CRISPR/Cas9 and pharmacological inhibition in *KRAS*-mutant, non-mutant cells. In addition, *Parp-1* knockout mice were combined with iCCA induction by hydrodynamic tail vein injection to evaluate an impact on phenotypic and molecular features of *Kras*-driven and *Kras*-wildtype iCCA. Clinical implications were confirmed in authentic human iCCA.

Results PARP-1 was significantly enhanced in *KRAS*-mutant human iCCA. PARP-1-based interventions preferentially impaired cell viability and tumourigenicity in human *KRAS*-mutant cell lines. Consistently, loss of *Parp-1* provoked distinct phenotype in *Kras/Tp53*-induced versus *Akt/Nicd*-induced iCCA and abolished *Kras*-dependent cholangiocarcinogenesis. Transcriptome analyses confirmed preferential impairment of DNA damage response pathways and replicative stress response mediated by CHK1. Consistently, inhibition of CHK1 effectively reversed PARP-1 mediated effects. Finally, *Parp-1* depletion induced molecular switch of *KRAS*-mutant iCCA recapitulating good prognostic human iCCA patients.

Conclusion Our findings identify the novel prognostic and therapeutic role of *PARP-1* in iCCA patients with activation of oncogenic *KRAS* signalling.

WHAT IS ALREADY KNOWN ON THIS TOPIC

⇒ PARP-1 is involved in multiple oncogenic pathways and processes, including DNA repair, genomic stability, chromatin modification, energy metabolism and apoptosis. Evidence suggests an association between *PARP-1* overexpression and *KRAS* mutations in various cancers, such as acute myeloid leukaemia and colorectal cancer. However, there is limited information available on the impact of *PARP-1* expression on therapeutic response in *KRAS*-mutant intrahepatic cholangiocarcinoma (iCCA).

WHAT THIS STUDY ADDS

⇒ Our results demonstrate that *KRAS*-mutant iCCA cells become highly sensitive to PARP-1 depletion and inhibition in vitro while Parp-1 deficient mice show reduced cholangiocarcinogenesis in vivo. Mechanistically, PARP-1 effects in *KRAS*-mutant iCCA are mediated through CHK1 activation, and this process can be reversed by chemical inhibition. Inhibiting PARP-1 in *KRAS*-mutant tumours leads to a favourable change in prognostic outcome for human iCCA.

HOW THIS STUDY MIGHT AFFECT RESEARCH, PRACTICE OR POLICY

⇒ These findings reveal a novel prognostic and therapeutic role of PARP-1 in iCCA patients with activated oncogenic KRAS signaling and poor prognosis. This knowledge may open new avenues for targeted therapies in this particular subset of iCCA patients.

INTRODUCTION

Intrahepatic cholangiocarcinoma (iCCA) is the second most common primary liver cancer (PLC) with increasing incidence and rising mortality rates.[1–3] A profound genetic heterogeneity and diverse spectra of prognostically distinct molecular subgroups render iCCA a prototype for precision oncological approaches.[4 5] Several druggable alterations in oncogenic signalling pathways (eg, *fibroblast growth factor receptor 2 gene* fusions,

isocitrate dehydrogenase 1 and 2 mutations) have been identified in iCCA. The application of specific inhibitors became a new mainstay of therapy and significantly improved the overall survival of patients. However, despite great progress in molecularly guided therapy, only 30%–40% of the iCCA patients present with the above-mentioned druggable alterations.[6] Thus, therapeutic options remain severely limited for the majority of patients. Among the most prominent alterations identified in iCCA, *KRAS* mutations historically posed significant challenges for specific targeting.[2 7] Activating *KRAS* mutations have been observed in around 10%–15% of iCCA patients. Importantly, *KRAS* alterations are characterised by poor response to commonly used chemotherapy and display a reduced overall survival.[8 9] Besides direct protumourigenic properties and increased proliferative characteristics, activated RAS-signalling results in increased intracellular stress which renders RAS-driven tumours particularly dependent on non-oncogenic mechanisms that promote oxidative stress response, apoptosis, and, particularly, DNA damage response (DDR).[10 11]

Several lines of evidence suggest that inhibition of the DDR protein PARP-1 might selectively affect the survival of *KRAS*-mutant tumour cells of different entities, including colorectal cancer (CRC) as well as acute myeloid leukaemia (AML).[12–14] PARP-1 is the most prominent member of the PARP family, involved in several cellular processes such as DDR, genomic stability, chromatin modification, transcription regulation, energy metabolism and programmed cell death. It catalyses poly(ADP-ribosyl)ation (PARylation) on metabolic, oxidative or genotoxic stress and influences the cellular metabolic status by enhancing NAD+ and ATP consumption.[15 16] Inhibition of PARP-1 is closely linked to the concept of synthetic lethality, as pharmacologically inactivated PARP-1 is trapped onto the DNA, causing stalling of the replication fork and thereby sensitising DDR-deficient cells.[17] Consequently, PARP-1 inhibitors have emerged as a therapeutic option in BRCA1/2-mutant ovarian and breast cancers, as well as in prostate and pancreatic cancer that depend on functional DNA repair mechanisms.[18 19] Several clinical trials evaluate PARP-1 inhibition in CCA, however, the mechanistic and therapeutic relevance of *PARP-1* and its inhibition in the context of *KRAS*-mutant iCCA is unknown.[20] In the presented study, we aimed to dissect phenotypic and molecular characteristics of *PARP-1* in iCCA with a particular focus on *KRAS*-mutant subgroups known to have a high cellular turnover (thus, constitutively activated DNA repair mechanisms).[10 11]

RESULTS

PARP-1 expression is abundant in *KRAS*-mutant iCCA

Given the relevance of deregulated DNA repair mechanisms in cholangiocarcinogenesis (particularly homologous recombination (HR) and non-homologous end-joining (NHEJ)), we sought to investigate the relationship between *KRAS* mutations and *PARP-1* expression (figure 1A).[12 13] First, we aimed to investigate a putative association between both molecules in iCCA tissue and analysed the correlation between *PARP-1* and *KRAS* expression in the TCGA patient cohort.[21 22] The median expression of *PARP-1* and *KRAS* was significantly upregulated in cholangiocarcinoma (CHOL) ($p<0.01$) (online supplemental figure S1A-C). Further, pairwise correlation analysis showed a positive correlation ($r=0.6$, $p<0.0001$) (online supplemental figure S1D,E) between both genes. Interestingly, while *PARP-1* expression was significantly upregulated in both iCCA and HCC, association with *KRAS* could only be confirmed in iCCA. To confirm these observations, we performed PARP-1 staining using a tissue microarray (TMA) comprising 194 iCCA as well as 54 specimens from normal bile ducts. We confirmed that PARP-1 levels were significantly increased in iCCA versus normal bile duct (online supplemental figure S1F, $p<0.0001$). In addition, we evaluated the expression of *PARP-1* in an independent iCCA cohort including 151 iCCA, 143 surrounding liver and nine normal bile ducts. Consistently, a significant upregulation of the *PARP-1* on a transcriptome level was observed in iCCA in comparison with the surrounding liver and normal bile ducts (online supplemental figure S1G). In addition, expression of *PARP-1* was positively correlated with genes known to be associated with proliferative capacity (online supplemental figure S1H). Interestingly, expression of *PARP-1* also showed a significant association with overall survival and recurrence-free survival based on *KRAS* status in iCCA (online supplemental figure S1I).

Next, we examined *PARP-1* expression in a variety of different *KRAS*-mutant and *KRAS*-wildtype iCCA cell lines. Consistently, we found a significant overexpression of *PARP-1* in *KRAS*-mutant iCCA cell lines versus non-mutant cell lines (CCC33 vs CCC16 $p=0.0240$; WITT vs HuCCT1 $p=0.0142$; WITT vs RBE $p=0.0034$; HuH28 vs HuCCT1 $p=0.0113$; HuH28 vs RBE $p=0.0023$) (figure 1B). Significant increase of PARP-1 could further be confirmed on protein level (CCC33 vs CCC16 $p=0.0286$; WITT vs HuCCT1 $p=0.0105$; WITT vs RBE $p=0.0122$; HuH28 vs HuCCT1 $p=0.0162$; HuH28 vs RBE $p=0.0234$) (figure 1C,D). Together, these investigations support the hypothesis that *PARP-1* is preferentially upregulated on RNA and protein level in *KRAS*-mutant, but not *KRAS*-wildtype iCCA.

KRAS-mutant iCCAs show preferential sensitivity towards *PARP-1* inhibition in vitro

Given the potential association of *KRAS* mutations and *PARP-1* overexpression in iCCA, we next employed selective RNAi knockdown of *PARP-1* in the *KRAS*-mutant and non-mutant iCCA cell lines to further characterise the potential of *PARP-1* as a putative therapeutic target in this subgroup of patients. Successful knockdown of PARP-1 protein expression was confirmed by Western blotting overall achieving a 66.6%–83.8% reduction compared with control cells (CCC33 78.5%, $p=0.0091$; CCC16 71.0%, $p=0.0040$; WITT 66.6%, $p=0.0358$; HuCCT1 82.4%, $p<0.0001$; RBE 83.8%, $p=0.0006$) (figure 1E). Importantly, PARP-2 protein levels were not affected by the PARP-1 knockdown. Notably, transfection of the *KRAS*-wildtype iCCA cell line HuH28 was not successful due to the low proliferation rate of this cell line. The impact of *PARP-1* knock-down on proliferation was subsequently demonstrated using CFU and SFU. A significant reduction of colony (CCC16 40.5%, $p=0.0043$; HuCCT1 38.8%, $p=0.0243$; RBE 40.4%, $p=0.0002$) and spheroid (CCC16 40.8%, $p=0.0041$; HuCCT1 41.5%, $p<0.0001$; RBE 46.7%, $p<0.0001$) formation capacity ranging from 35.6% to 45.8% was observed in *KRAS*-mutant versus control cells. In contrast, neither colony nor spheroid formation capacity was affected in *KRAS*-wildtype iCCA cell lines (figure 1F).

Next, we used the FDA-approved PARP-1 inhibitor olaparib to confirm the association of PARP-1 and KRAS in the context of chemical inhibition. In concordance with the finding from RNAi experiments, *KRAS*-mutant iCCA cell lines showed a significantly reduced viability in response to PARP-1 inhibition compared with *KRAS*-wildtype cell lines (CCC33 vs CCC16 $p=0.0068$; WITT vs HuCCT1 $p=0.0078$; WITT vs RBE $p=0.0026$; HuH28 vs HuCCT1 $p=0.0725$; HuH28 vs RBE $p=0.0114$) (online supplemental figure S2A). Moreover, olaparib caused

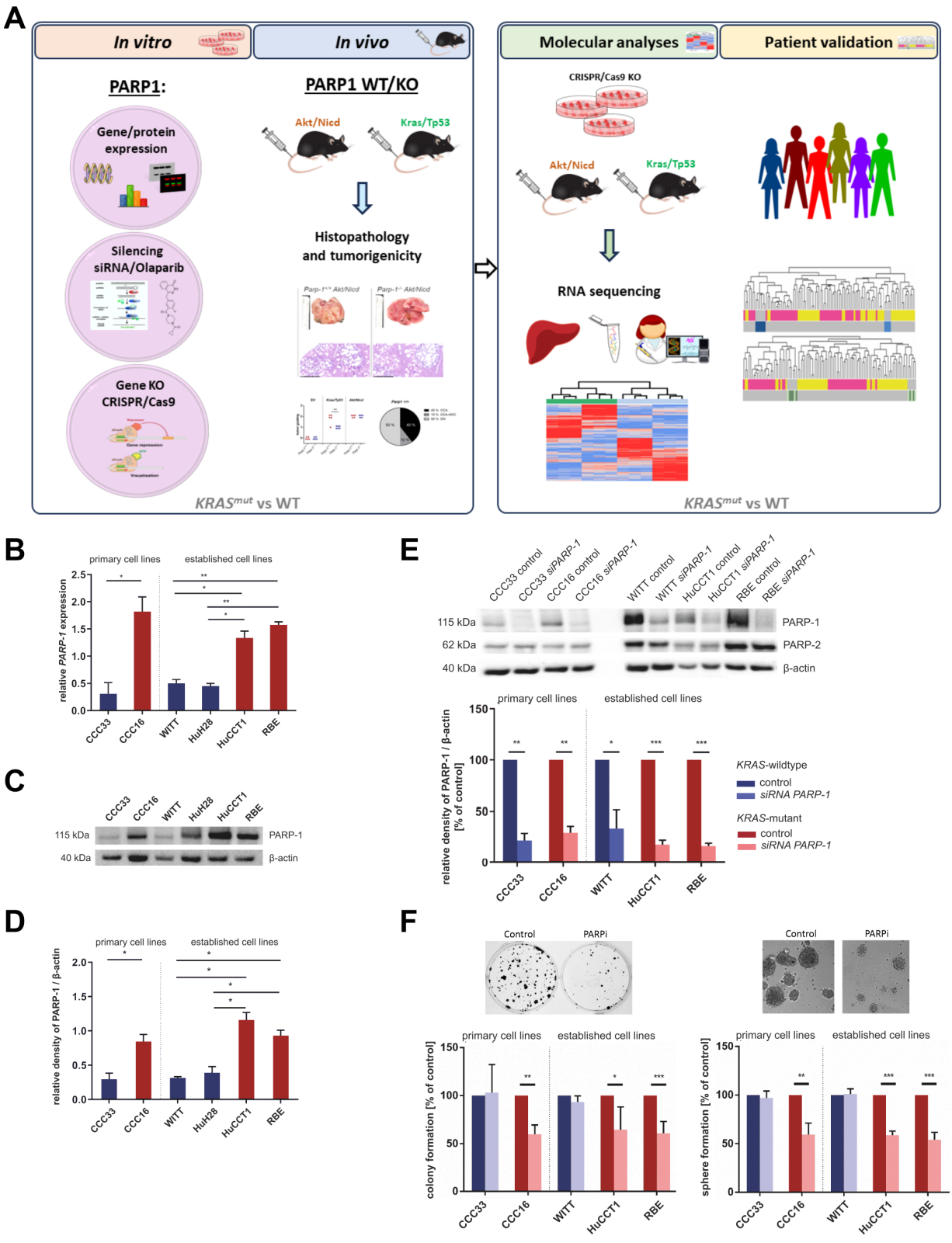

Figure 1 PARP-1 expression in *KRAS*-mutant and *KRAS*-wildtype iCCA and effect of siRNA-mediated knockdown of *PARP-1* on cell viability, colony and sphere formation capacity. (A) Graphical representation of the experimental design. (B) Relative *PARP-1* expression normalised to normal liver tissue in *KRAS*-mutant (CCC16, HuCCT1, RBE; red) and *KRAS*-wildtype iCCA cell lines (CCC33, WITT, HuH28; blue). Mean±SD, n=3, *p<0.05, **p<0.01. (C) Representative Western blot and (D) densitometry analysis of basal PARP-1 protein expression in *KRAS*-mutant and *KRAS*-wildtype iCCA cell lines. Relative density of PARP-1 expression normalised to β-actin is shown. Mean±SD, n=3, *p<0.05. (E) Representative Western blot and densitometric analysis of siRNA-mediated knockdown of PARP-1 protein expression in *KRAS*-mutant (CCC16, HuCCT1, RBE; red) and *KRAS*-wildtype iCCA cell lines (CCC33, WITT; blue). Relative density of PARP-1 expression normalised to β-actin is shown. Mean±SD, n=3, *p<0.05, **p<0.01, ***p<0.001. (F) Representative images of colony and sphere formation assay as well as % of control after siRNA-mediated *PARP-1* knockdown in *KRAS*-mutant and *KRAS*-wildtype iCCA cell lines. Mean±SD, n=3, *p<0.05, **p<0.01, ***p<0.001. iCCA, intrahepatic cholangiocarcinoma.

a selective G1 cell cycle arrest in *KRAS*-mutated primary cells (online supplemental figure S2B).

In addition, PARP-1 inhibition also led to a decrease in the number of CFU and SFU in *KRAS*-mutant iCCA cell lines (CFU: CCC16 50.3%, p=0.0003; HuCCT1 51.6%, p<0.0001; RBE 49.6%, p<0.0001; SFU: CCC16 36.6%, p<0.0001; HuCCT1 38.5%, p=0.0002; RBE 42.1%, p<0.0001). Although olaparib exerted slight effects on colony formation in *KRAS*-wildtype iCCA cell lines CCC33 (27.6%, p=0.0003) and WITT (8.4%, p=0.0171), the spheroid forming capacity of *KRAS*-wildtype iCCA cell lines remained unaffected in all cell lines on olaparib treatment (online supplemental figure S2C). Notably, reduction in CFU was considerably less pronounced in *KRAS*-wildtype versus *KRAS*-mutant cells, which is presumably due to unspecific toxic effects of olaparib unrelated to PARP-1 inhibition.

To unveil potential synergistic effects between olaparib and cytotoxic compounds used for iCCA therapy, we treated KRAS-wildtype and mutated primary cell lines (CCC16 and CCC33) with olaparib in combination with cisplatin and gemcitabine. Combination therapy showed a significantly higher level of synergism for both tested drugs, gemcitabine and cisplatin, in the *KRAS*-mutated cell line (online supplemental figure S2D). To further address whether inhibition of other components of the DDR would induce a similar selective response in *KRAS*-mutated cancers, we tested the efficacy of an additional drug involved in DDR, namely the DNA-PKcs inhibitor KU57788, leading to inhibition of NHEJ. Consistent with a selective effect of PARP-1 inhibition in *KRAS*-mutated iCCA, effect of KU57788 was independent of the mutational status and no significant differences between *KRAS* WT and KO cell lines were observed (online supplemental figure S2E). Taken together, these investigations confirm the preferential antitumourigenic effects of PARP-1-based interventions in *KRAS*-mutant iCCA cell lines and validate the potential utility of combination therapy for the treatment of this subtype of iCCA.

Impact of *PARP-1* depletion on transcriptomic profile, DDR and ROS in *KRAS*-mutant iCCA cell lines

Our functional analyses showed pronounced *KRAS*-dependent differences in iCCA cell lines on PARP-1-based interventions. To further define molecular alterations influenced by PARP-1 inhibition, we generated stable *PARP-1* knockout (*PARP-1* KO) clones of the different iCCA cell lines HuCCT1, RBE, WITT and CCC33 using CRISPR/Cas9 followed by RNA sequencing (online supplemental figure S3A).

First, we explored whole transcriptome differences in *PARP-1* KO in *KRAS*-mutant iCCA cell lines compared with their scrambled control clones using Wald's statistics and revealed a total of 1171 (660 down, 511 up) differentially expressed genes (p<0.05; online supplemental table S1). Accordingly, unsupervised hierarchical cluster analyses and principal component analysis plot confirmed that *PARP-1* KO clones of both *KRAS*-mutant iCCA cell lines display distinct molecular profiles (figure 2A).

We also evaluated functional signalling pathways related to the differential response to *PARP-1* deficiency and identified that gene sets related to cell cycle control, for example, G1/S checkpoint regulation as well as BRCA1-mediated DNA damage, among others, were significantly dysregulated after *PARP-1* KO (figure 2B). In addition, oxidative stress response (NRF-2 mediated oxidative stress response, HIF1α signalling) as well as apoptosis-related pathways (death receptor signalling, apoptosis signalling, Necroptosis signalling, and Myc-mediated apoptosis) were affected by selective depletion of *PARP-1* in *KRAS*-mutant iCCA cells (figure 2B). Further, the cell lines also showed disruption in known oncogenic signalling resembling ERK/MAPK, p53, HIF1α and NF-κB signalling after *PARP-1* depletion. Moreover, *PARP-1* KO enhanced adverse processes in *KRAS*-mutant iCCA cell lines (online supplemental figure S4A), known to promote hepatobiliary carcinogenesis. Consistently, gene sets related to DNA repair mechanisms, such as the G2/M DNA damage checkpoint and BER, apoptosis and TGFβ signalling were significantly enriched in *KRAS*-mutant *PARP1* KO cells (online supplemental figure S4B). Overall, transcriptomic analyses indicated a dependency of *KRAS*-mutant iCCA cells on functional DNA repair mechanisms to compensate for increased oxidative stress, apoptotic stimuli and replicative stress induced by a high cellular turnover and proliferative capacity of *KRAS*-mutant iCCA cell lines on *PARP-1* KO, which might confer the distinct effects in *KRAS*-mutant iCCAs.

We further evaluated the impact of irradiation and oxidative stress on *KRAS*-mutant and *KRAS*-wildtype iCCA cell lines on *PARP-1* KO. First, we investigated the impact of irradiation-induced DNA damage in *PARP-1* KO clones by measuring phospho-γH2AX foci as a marker for DNA double-strand breaks. Irradiation led to a significantly increased number of DNA double-strand breaks in *KRAS*-mutant iCCA cell line RBE only in *PARP-1* KO clones compared with control conditions (online supplemental figure S5A). In contrast, *KRAS*-wildtype iCCA cell line CCC33 showed a significantly increased number of DNA double-strand breaks independent of *PARP-1* KO status. Assessment of ROS level showed that in *KRAS*-mutant iCCA cell line RBE the basal ROS levels were significantly higher in the *PARP-1* KO clones when compared with their respective scrambled control clones. In contrast, the basal status of ROS did not differ in *PARP-1* KO clone of *KRAS*-wildtype iCCA cell line CCC33. Consistently, H_2O_2 administration led to a significant increase in oxidative stress in *KRAS*-mutant iCCA cell lines, whereas levels of oxidative stress in *KRAS*-wildtype iCCA cell line CCC33 remained unaffected (online supplemental figure S5B).

Mechanism of PARP-1 regulation was further explored in authentic iCCA tumours harbouring *KRAS* mutation. *KRAS*-mutated iCCA showed upregulation of genes associated with DNA double-strand break repair mechanisms. In addition, genes associated with HR (eg, *BARD1, EXO1, RAD54L, CHEK1, UIMC1, RAD51, BRCA2*) and both canonical and alternative NHEJ (c-NHEJ; eg, *XRCC4, DCLRE1C*; alt-NHEJ; eg, *POLQ, LIG1, FEN1, XRCC1*) were activated (online supplemental figure S5C). We further tested enrichment of gene sets in *KRAS*-mutant tumours to test association with PARP-1 and DNA damage control. Analyses revealed enrichment of BRCA1 and HR in the tumours carrying *KRAS* mutation (online supplemental figure S5D). To substantiate these observations, we performed RPPA analyses of two primary cell lines representing the mutational *KRAS* status and confirmed that proteins involved in HR are significantly increased in *KRAS*-mutated cells (CCC16) (CtIP, RAD50 and RAD51) (online supplemental figure S5E). Thus, these investigations underline that major mechanisms of DNA damage repair, including *PARP-1*, are closely associated with *KRAS* mutation in iCCA.

In addition, we preformed single-cell analysis of tumours from 11 iCCA patients. These analyses confirmed differential expression of DDR genes in malignant cells from patients with *KRAS* mutations compared with those cells derived from patients without the mutations. This was not observed in non-malignant cells, suggesting that the phenomenon is tumour cell specific (online supplemental figure S6A-C).

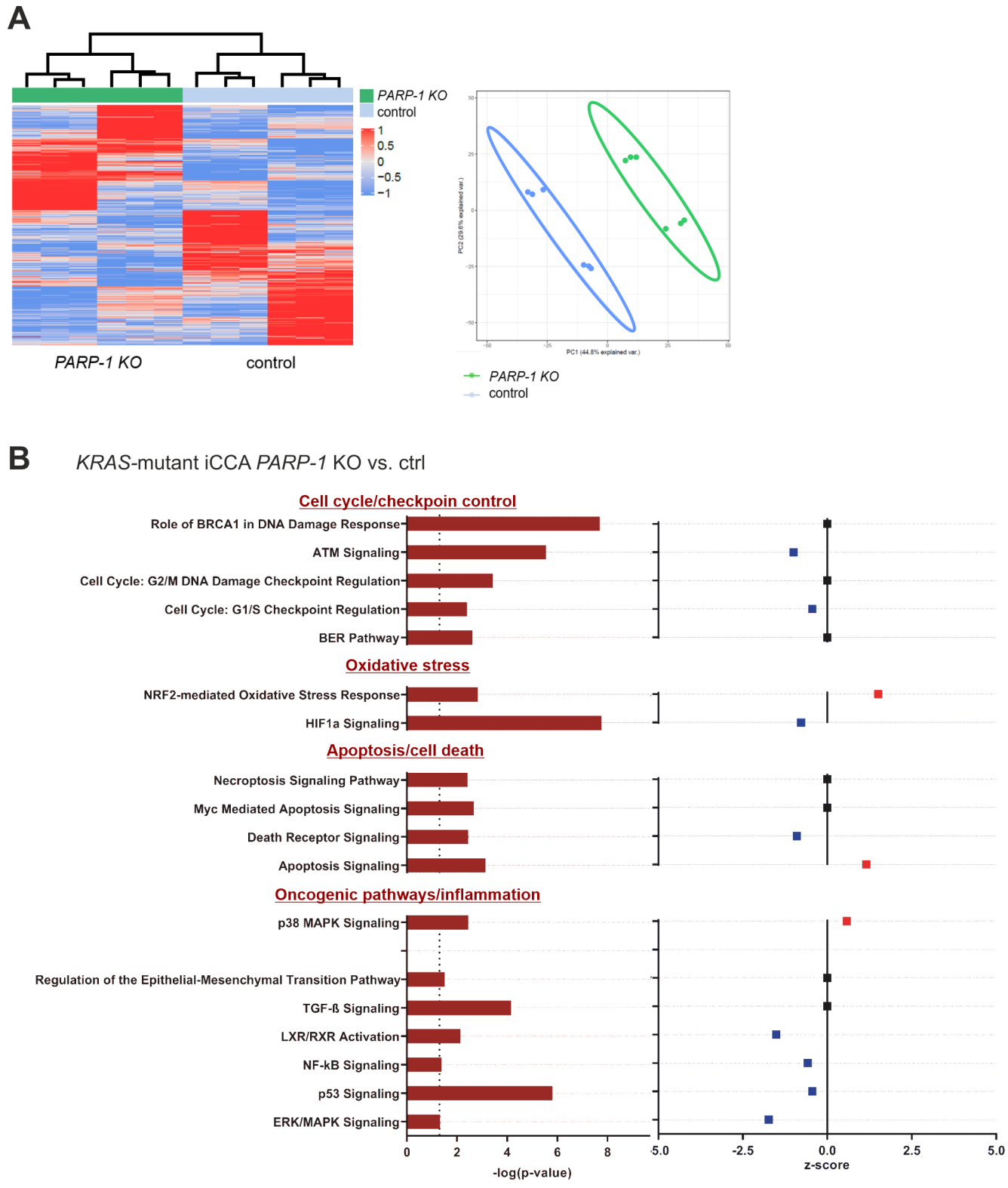

Figure 2 Differential gene expression in *KRAS*-mutant iCCA cell lines on *PARP-1* KO. (A) Unsupervised cluster and PCA of significant genes (p<0.05) of *KRAS*-mutant iCCA cell lines (HuCCT1, RBE) on *PARP-1* KO versus control. (B) Canonical pathways significantly regulated in *KRAS*-mutant iCCA cell lines on *PARP-1* KO versus control identified by IPA. The dashed line indicates the significance threshold of –log (p value >1.3). Shown are z-scores of respective canonical pathways (positive z-score=red/activated, negative z-score=blue/inhibited). iCCA, intrahepatic cholangiocarcinoma; IPA, ingenuity pathway analysis; PCA, principal component analysis.

Hepatobiliary carcinogenesis is selectively impaired in *Kras/Tp53*-driven tumours with genetic *Parp-1* deficiency

To dissect the relevance of *PARP-1* in *KRAS*-driven and non-*KRAS*-mutant iCCA development, we employed HDTV-induced hepatobiliary carcinogenesis in genetically modified *Parp-1* proficient and deficient mice. Herein, *Kras* induction

together with *Tp53* knockdown (*Kras*/*Tp53*) led to preferential occurrence of distinct solid tumours within 10 weeks after injection in *Parp-1* proficient mice (online supplemental figure S7A). Histopathological analyses of an expert hepatopathologist revealed tumours with gland-like structures in accordance with the diagnosis of iCCA, most often well differentiated, in one example also with signs of dedifferentiation with sarcomatoid tumour cells including tumour giant cells (figure 3A, online supplemental figure S8A). No mucin production was observed, that is, the tumours resemble iCCA of small-duct type. In addition, *Parp-1* proficient mice also displayed multiple small-cell dysplastic foci and nodules with development of early hepatocellular carcinoma and focal tumourous vein invasion (online supplemental figure S8B).

In striking contrast, animals with *Parp-1* deficient genotype were characterised by a complete absence of CCA features. Histopathological assessment revealed multiple, diffuse hepatocellular carcinomas as well as dysplastic nodules with focal tumourous vein invasion (figure 3A). Further, moderate macrovesicular steatosis (11%–50%) and disrupted architecture of liver parenchyma was also observed (online supplemental figure S8A,B). These investigations suggest that the *Parp-1* deficiency preferentially inhibits cholangiocarcinogenesis.

Mice with tumours induced by *Kras*/*Tp53* combination showed significant differences in their average body weight between *Parp-1*$^{+/+}$ and *Parp-1*$^{-/-}$ animals with 27.8 g and 29.7 g, respectively (p=0.0234). Further, the average liver weight significantly differed depending on the *Parp-1* status with 2.75 g for *Parp-1*$^{+/+}$ and 6.10 g for *Parp-1*$^{-/-}$ mice (p<0.0001), likely due to the presence of tumour nodules (online supplemental figure S7B). Consistently, we observed pronounced differences in liver to body weight (L/B)-ratio and scoring on *Kras*/*Tp53* injection between *Parp-1*$^{+/+}$ and *Parp-1*$^{-/-}$ experimental groups (L/B-ratio p<0.0001, tumour scoring p=0.003) (figure 3B-D).

Interestingly, classic biliary marker (Sox9) confirmed cholangiocarcinoma in tumour sections of *Parp-1*$^{+/+}$ mice injected with *Kras*/*Tp53*, whereas dysplastic nodules in surrounding liver sections of *Parp-1*$^{+/+}$ mice as well as of *Parp-1*$^{-/-}$ mice were expectedly negative for Sox9 expression, confirming the hepatocellular lineage of these cells (figure 3A). Nuclear Parp-1 expression was detectable in all sections of *Parp-1*$^{+/+}$ mice, whereas no Parp-1 expression was determined in *Parp-1* deficient liver sections (*Parp-1*$^{+/+}$ tumour vs *Parp-1*$^{-/-}$ dysplastic foci p<0.0001; *Parp-1*$^{+/+}$ dysplastic foci vs *Parp-1*$^{-/-}$ dysplastic foci p<0.0001) (online supplemental figure S9A). As expected, significantly higher proliferation (Ki67) was detected in tumour tissue of *Parp-1* proficient mice compared with dysplastic nodules (*Parp-1*$^{+/+}$ tumour vs *Parp-1*$^{+/+}$ dysplastic foci p<0.0001; *Parp-1*$^{+/+}$ tumour vs *Parp-1*$^{-/-}$ dysplastic foci p<0.0001) (online supplemental figure S9A). Further, DNA damage sites represented by γH2ax positive foci were randomly distributed in both tumour and surrounding liver sections of *Parp-1*$^{+/+}$ mice and significantly more pronounced than in *Parp-1*$^{-/-}$ mice (*Parp-1*$^{+/+}$ tumour vs *Parp-1*$^{-/-}$ dysplastic foci p<0.0001; *Parp-1*$^{+/+}$ dysplastic foci vs *Parp-1*$^{-/-}$ dysplastic foci p=0.009) (online supplemental figure S9A). Taken together, the histopathological assessment of the *Kras*/*Tp53*-induced tumours showed differences in tumour entity from the evolution of cholangiocellular carcinoma instead of hepatocellular carcinoma, confirming that iCCA development in *Kras*-mutant cancers is highly dependent on proficient *Parp-1* signalling.

To confirm the relevance of activated *Kras* in a *Parp-1* deficient background, non-*Kras*-driven iCCAs were induced by myrAkt/myc-tagged Nicd (combination referred to as *Akt*/*Nicd*). Average body and liver weight did not differ significantly dependent on the *Parp-1* genotype in the *Akt*/*Nicd* model (online supplemental figure S7B). Further, animals injected with *Akt*/*Nicd* developed tumours and cystic alterations 7 weeks after HDTV with pronounced hepatomegaly as well as steatohepatitis independent of the *Parp-1* genotype (figure 3A, online supplemental figure S8A). An expert pathologist classified the tumours as iCCA with well to moderate differentiation grade (G1–2), severe macrovesicular steatosis (>50%) and disrupted architecture of liver parenchyma due to the occurrence of multiple tumour foci (online supplemental figure S8B). Sporadic or unspecific effects of HDTV were excluded in livers of mice injected with empty vector (EV) control (results not shown). In contrast to *Kras*/*Tp53*-induced hepatobiliary tumour growth, EV-injected and *Akt*/*Nicd*-injected animals showed no differences in morphology, histological classification and quantification (L/B-ratio, tumour scoring) of tumours/livers (figure 3B–D, online supplemental figures S8A,B and S9B). Thus, a selective effect of *Parp-1* depletion in *Kras*/*Tp53*-driven tumours was confirmed.

Impact of *Parp-1* deficiency on the transcriptome of *Kras*/*Tp53*-induced cholangiocarcinogenesis via HDTV

To further define the molecular features underlying distinct morphological and histopathological differences in the groups, we performed RNA sequencing of HDTV-induced tumours driven by *Kras*/*Tp53* or *Akt*/*Nicd*.

We identified a total of 7661 differentially expressed genes (4577 downregulated, 3084 upregulated) between liver/tumour tissue samples of *Kras*/*Tp53 Parp-1*$^{+/+}$ and *Parp-1*$^{-/-}$ animals (p<0.05) (figure 4A; online supplemental table S2). Pathways related to cell cycle control, like G1/S checkpoint regulation and G2/M DNA damage checkpoint regulation and ATM signalling were among the prominent molecular changes associated with the phenotype (figure 4B, online supplemental figure S10). Further, the DNA double-strand break repair pathway associated with BRCA1 was predicted to be negatively regulated in *Parp-1* deficient animals versus *Parp-1* proficient animals. These findings suggest that DDR mechanisms are dysregulated in *Kras*/*Tp53*-injected animals in a *Parp-1*-dependent manner. Further functional networks involved inhibition of oxidative stress pathways (NRF-2-mediated oxidative stress response, HIF1α signalling), whereas apoptosis-related pathways were activated (death receptor signalling) in *Parp-1* deficient animals. *Kras*/*Tp53* induced tumours under *Parp-1* KO showed enrichment of LXR/RXR, p53, PTEN and HIPPO signalling. Inhibition of pathways was shown in key oncogenic pathways like TGFβ, NF-κB, Notch and ERK/MAPK signalling (figure 4B). Interestingly, several DNA repair pathways were significantly enriched in *Parp-1*$^{+/+}$ mice injected with *Kras*/*Tp53*. Besides DNA single-strand break repair mechanisms, also double-strand break repair pathways (NHEJ, HR) were enriched suggesting that *Parp-1* proficiency is important for DDR and repair mechanisms in *Kras*-driven hepatobiliary tumourigenesis (online supplemental figure S11A). Activation of key pathways identified at the transcriptomic level was validated by IHC in *Kras*/*Tp53 Parp-1*$^{-/-}$ animals (online supplemental figure S10C). These findings are in concordance with our in vitro findings (figure 2, online supplemental figure S4).

To confirm the selective effects of *Kras* in *Parp-1* deficient animals, we analysed transcriptomic profiles of *Parp-1* deficient and proficient mice injected with *Akt*/*Nicd*. The number of significantly altered genes was considerably less, comprising only 158 (95 down, 63 up) differentially expressed genes (p<0.05)

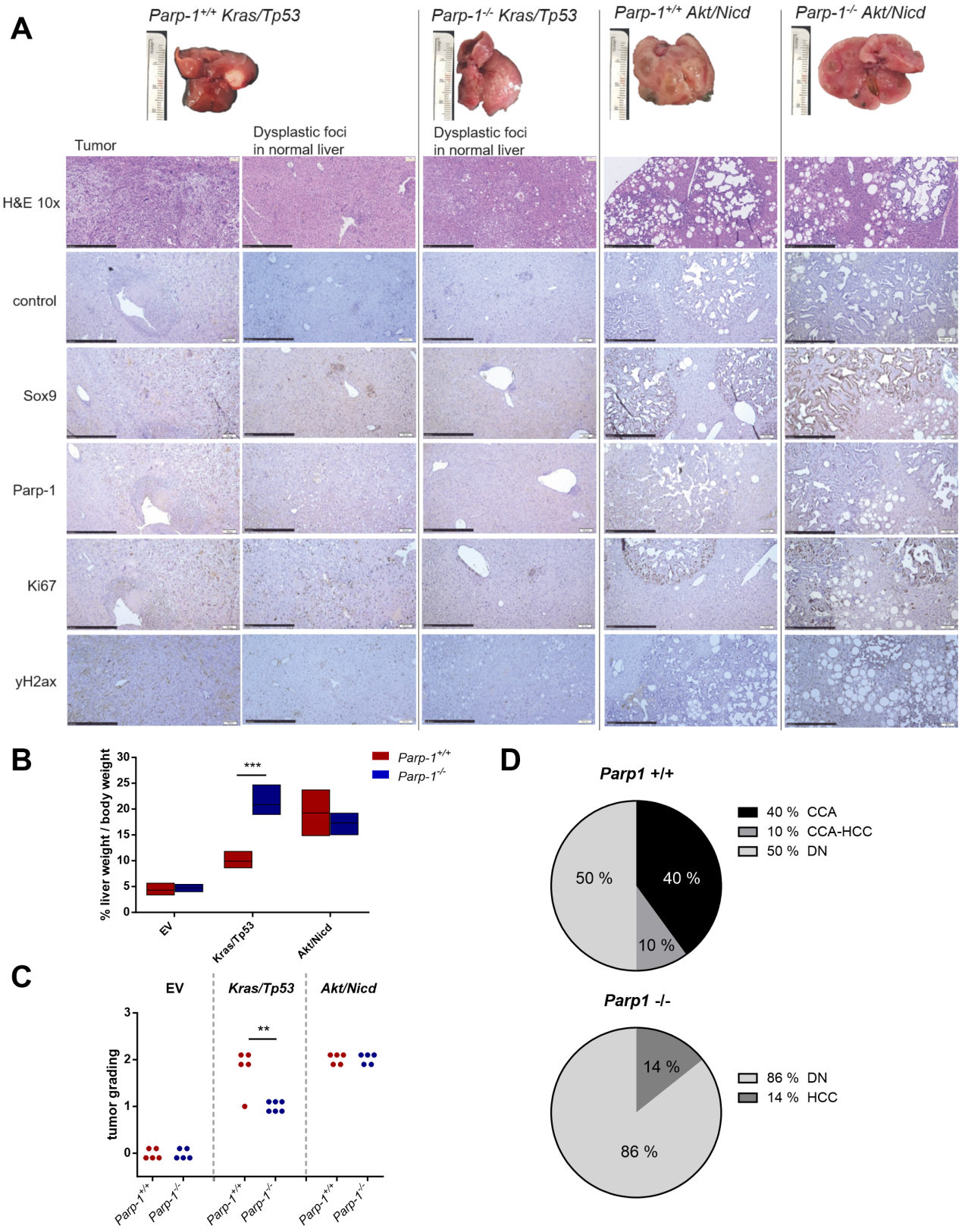

Figure 3 Histology and immunohistochemistry (IHC) of liver sections injected with *Kras/Tp53* via HDTV and *Akt/Nicd* via HDTV and quantification of in vivo tumour growth. (A) Representative images of livers with tumour induction via HDTV (*Kras/Tp53; Akt/Nicd*) in *Parp-1*$^{+/+}$ (n=5/6) and *Parp-1*$^{-/-}$ mice (n=6). H&E and IHC staining of selected proteins (Sox9, Parp-1, Ki67 and γH2ax) of representative paraffin-embedded tumour sections are shown (3.5 µm). Scale bars indicate 500 µm (×10, H&E) and 1000 µm (×5, IHC). (B) Liver weight/body weight ratio (%) of *Parp-1*$^{+/+}$ mice (blue) and *Parp-1*$^{-/-}$ mice (red) after HDTV of empty vector (EV), *Akt/Nicd* or *Kras/Tp53* plasmid combinations with HSB2. Mean±SD, n=5, **p<0.01, ***p<0.001. (C) Quantification of tumour growth shown as scores: 0=no tumour, 1=small foci/nodules, 2=distinct solid tumour. EV n=5, *Akt/Nicd* n=5, *Kras/Tp53* n=5/6, **p<0.01. (D) Percentage of different lesions in *Parp-1*$^{+/+}$ and *Parp-1*$^{-/-}$ mice with *Kras/Tp53* plasmid combination. HDTV, hydrodynamic tail vein.

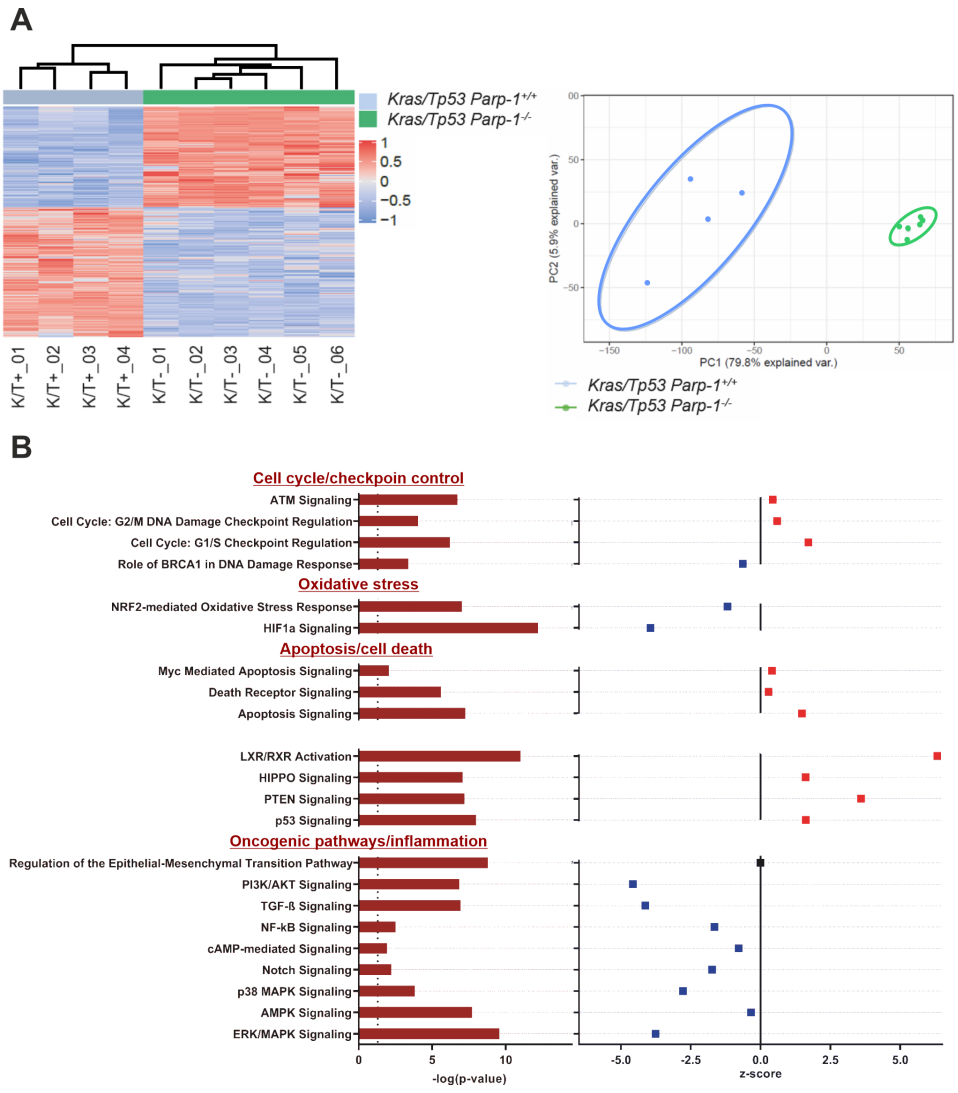

Figure 4 Differential expressed genes after HDTV with *Kras/Tp53* in *Parp-1*$^{-/-}$ versus *Parp-1*$^{+/+}$ mice. (A) Unsupervised cluster and PCA plot of significant genes (p<0.05) after HDTV with *Kras/Tp53* in *Parp-1*$^{-/-}$ versus *Parp-1*$^{+/+}$ mice. (B) Canonical pathways significantly regulated in tumours induced with *Kras/Tp53* in *Parp-1*$^{-/-}$ versus *Parp-1*$^{+/+}$ mice identified by IPA. Dashed line indicated significance threshold of –log (p value >1.3). Shown are z-scores of respective canonical pathways (positive z-score=red/activated, negative z-score=blue/inhibited). HDTV, hydrodynamic tail vein; IPA, ingenuity pathway analysis; PCA, principal component analysis.

vs 7661 in *Kras/Tp53* (online supplemental figures S12 and S13; online supplemental tables S2 and S3). These findings are in concordance with the equivalent tumour growth and histopathological features of *Akt/Nicd*-induced cholangiocarcinogenesis independent of the *Parp-1* genotype (figures 3 and 4, online supplemental figure S12). However, several components of DNA repair pathways of DSB repair (NHEJ, HR) showed upregulated expression in *Parp-1* proficient mice injected with *Akt/Nicd* confirming that the role of *Parp-1*, although important for DNA damage control, is independent of cholangiocarcinogenesis in *Akt/Nicd* experimental group.

Mechanisms of *PARP-1* activation in KRAS-mutated iCCA

Transcriptome analyses confirmed preferential impairment of cell cycle regulation, DDR pathways and replicative stress response in human iCCA cells, mouse model, as well as patient samples harbouring *KRAS* mutation. To elucidate the molecular mechanisms underlying the selective impairment of these pathways in KRAS-mutant iCCA, we first examined the expression of DDR genes in *Kras*-mutant and wild-type animals with functional *Parp-1*. Genes associated with HR, c-NHEJ and alt-NHEJ were significantly upregulated. In addition, a dominant activation of *Chk1* expression was observed. Interestingly, on Parp-1 inhibition in *Kras*-mutant animals, the expression of *Chk1* was also downregulated, suggesting an important relevance for Chk1 kinase in *Kras*-mutated iCCA (figure 5A). We further used GSEA in our different datasets to investigate molecular differences in *KRAS*-mutated and wildtype iCCAs. Commonly enriched set of genes across iCCA models encompassed cell cycle regulation and activation of E2F targets, G2M and spindle checkpoint activation, as well as DNA-damage repair via HR. Importantly, we have consistently observed activation of gene sets associated with CHK1/CHK2, key regulators of the cell cycle and cell survival (figure 5B). We further recognised that *CHK1* was highly expressed in iCCA but not normal liver tissue and showed a significant upregulation predominantly in *KRAS*-mutated cancers (figure 5C). Accordingly, public data also show a significant correlation of *CHK1* and *PARP-1* suggesting a regulatory network in *KRAS*-mutated iCCA that might be induced by the high replicative stress in this subgroup of tumours.

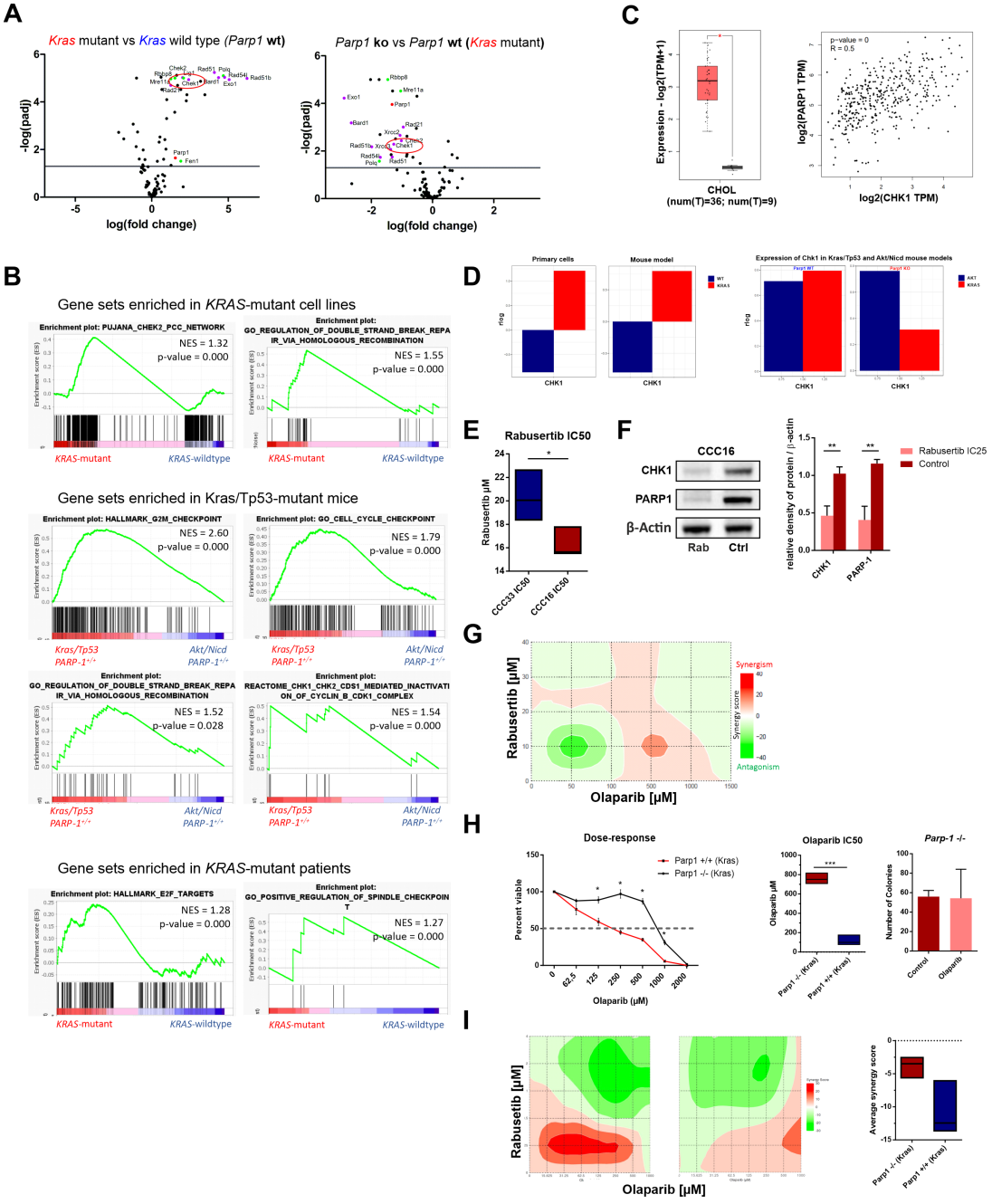

Figure 5 Molecular mechanisms of *PARP-1* regulation in *KRAS*-mutated iCCA. (A) Expression of DNA damage response genes including *Chk1* in *Parp-1*$^{-/-}$ and *Parp-1*$^{+/+}$ mice after *Kras/Tp53* injection. Volcano plots are depicted with the log (fold change) of each gene and the –log (p adjusted) was calculated by performing Wald test. Selected genes associated with HR, c-NHEJ and alt-NHEJ are coloured and gene names are displayed. Expression of *Chk1* is depicted with red ellipse (B) Gene set enrichment analysis (GSEA) in *KRAS*-mutated cell lines, *Kras/Tp53 Parp-1*$^{+/+}$ mouse model and patient samples. The selection of gene sets was based on statistical significance calculated by nominal p<0.05 and FDR<0.25. NES indicates the degree of overexpression for each group at the peak of the entire gene set. (C) *CHK1* gene expression profiles (TCGA) in cholangiocarcinoma versus normal liver tissue (CHOL) presented in box plots and correlation between *PARP-1* and *CHK1*. Values of *p<0.05 were considered as of significant difference. (D) Upper graphs depict gene expression level of *CHK1* in *KRAS*-mutated cell lines and *Kras/Tp53 Parp-1*$^{+/+}$/wildtype mouse model, Lower graphs show expression of *Chk1* in *Kras/Tp53* and *Akt/Nicd* mouse model with *Parp-1*$^{+/+}$ and *Parp-1*$^{-/-}$ genotype. (E) Shown are IC50 concentrations of Rabusertib for *KRAS*-mutated and non-mutated primary iCCA cell lines. Mean±SD, n=3, *p<0.05. (F) Representative Western blot and densitometric analysis of CHK1 and PARP-1 protein expression on treatment with IC25 concentration of Rabusertib in *KRAS*-mutant iCCA cell line. Relative density of PARP-1 expression normalised to β-actin is shown. Mean±SD, n=3, *p<0.05, **p<0.01, ***p<0.001. (G) Evaluation of synergistic or antagonistic effects between Rabusertib/Olaparib in primary human cell line. Plots indicate level of synergism between investigated drugs, where red colour represents synergism and green colour antagonism. (H) Dose-response curves of *Kras*-mutant mouse cell lines with and without functional Parp-1 treated with increasing concentrations of olaparib (left) and their respective IC50 values (middle). Right is shown total number of colonies with and without olaparib treatment. Mean±SD, n=3, *p<0.05. (I) Evaluation of synergistic or antagonistic effects between rabusertib/olaparib in mouse cell lines. Plots indicate level of synergism between investigated drugs, where red colour represents synergism and green colour antagonism. On the right, graph shows average synergy score (ZIP) for both cell lines. iCCA, intrahepatic cholangiocarcinoma; NHEJ, non-homologous end-joining.

Significant upregulation of *CHK1* was further demonstrated in our *KRAS*-mutated cell lines and *Kras/Tp53 Parp-1*$^{+/+}$ mouse model (figure 5D). As already demonstrated for PARP-1 inhibition, *KRAS*-mutated iCCA cells were significantly more sensitive to specific inhibition of CHK1 by the selective CHK1 inhibitor Rabusertib (figure 5E). Inhibition of CHK1 also led to a significant downregulation of PARP-1 while combined treatment with olaparib did not induce synergistic effects (figure 5F,G). Gene expression analysis following CHK1 inhibition showed upregulation of *CDC25C* and downregulation of *RAD51* and *XRCC2*, which could be actors of PARP-1 regulation in *KRAS*-mutated iCCAs. Interestingly, protein–protein interaction confirmed an association of these proteins with PARP-1 (online supplemental figure S14). Lastly, we tested the effect of Olaparib alone and in combination with rabusertib using an ex vivo model of primary cell lines derived from *Parp-1*$^{-/-}$ *Kras/Tp53* and *Kras*^{G12D}*;Rb*^{del}*;Tp53*^{del}. As expected, cell lines with *Kras* mutation and functional Parp-1 showed significantly higher sensitivity to Parp-1 inhibition while the observed synergistic effects in both cell lines were negative. Colony formation analysis in *Kras/Tp53 Parp-1*$^{-/-}$ after exposure to the IC50 concentration of olaparib unveiled that the number of colonies in the treatment was not significantly different from the control (figure 5H,I). The observed findings confirm that CHK1 has a profound effect on PARP-1 levels in this subtype of highly replicative cancers and contributes to the dependence of *KRAS*-mutated iCCA on functional PARP-1 signalling.

PARP-1 expression as prognostic factor in *KRAS*-mutant iCCA

To evaluate a potential prognostic impact of our molecular profiles, we integrated our identified in vitro and in vivo transcriptomic profiles with different established prognostic subgroups of PLC (poor and good prognosis).[8] Consistently, *KRAS*-mutant CRISPR/Cas9-mediated *PARP-1* KO clones grouped with good prognosis CCA patients, whereas *KRAS*-mutant control clones recapitulated transcriptomic features of poor prognosis CCA patients (figure 6A). Similarly, integration of in vivo data showed that *Parp-1* deficient mice with *Kras/Tp53* injection clustered with a good prognosis while *Parp-1* proficient mice grouped with poor prognosis (figure 6B). Importantly, mice injected with *Akt/Nicd* revealed no distinct clustering dependent on the *Parp-1* genotype (figure 6B). Overall, these results suggest that *PARP-1* depletion in iCCA with activated *KRAS* mutations leads to a shift from poor to good prognosis.

DISCUSSION

Recently, the PARP family has gained attention in cancer research due to its involvement in various oncogenic pathways and processes (DNA repair, genomic stability, chromatin modification, energy metabolism, apoptosis) mediated by the family members.[23] Elevated *PARP-1* expression was consistently observed in a variety of solid tumours.[24–28] Further, recent evidence suggests an association between *PARP-1* overexpression and *KRAS* mutations in different tumours, including in AML and CRC models.[12 13 29] However, until now, only very limited

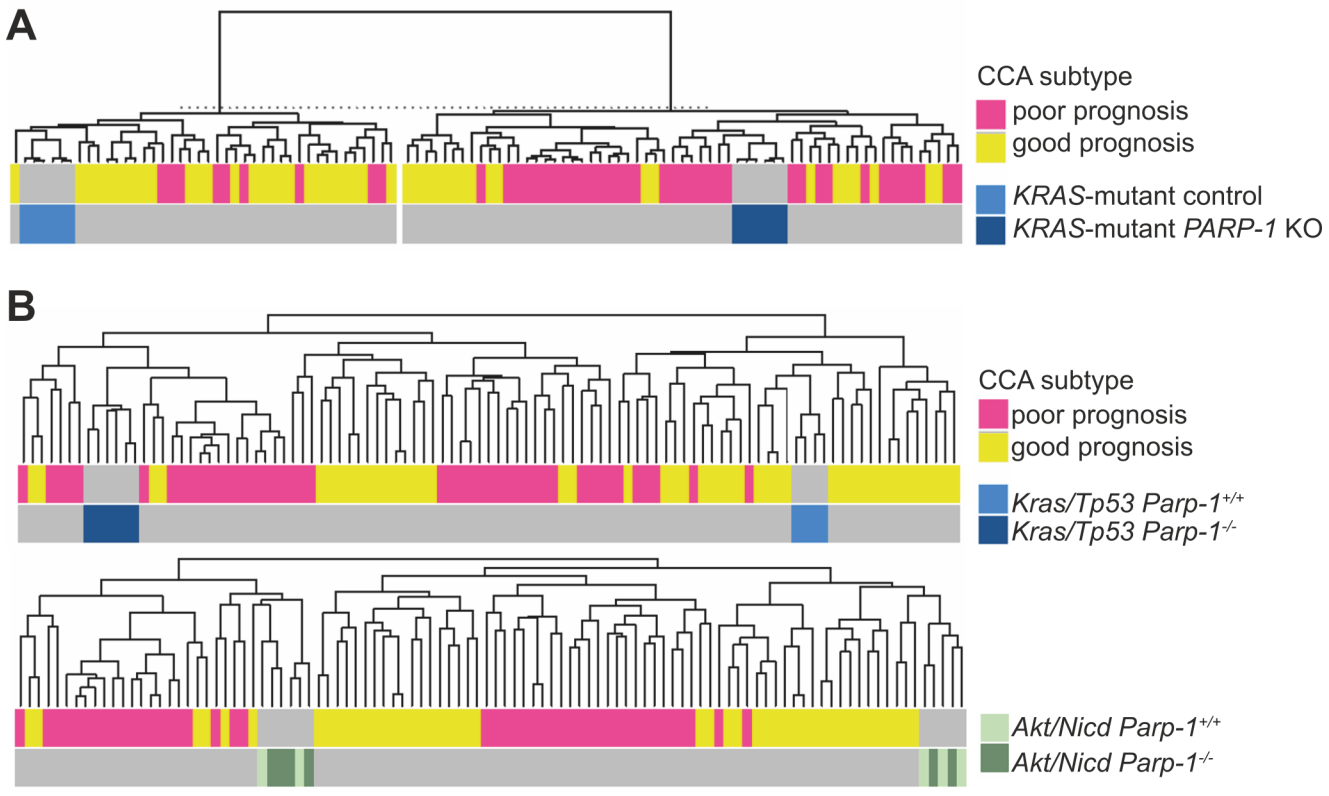

Figure 6 Integration of in vitro and in vivo transcriptomic data with prognostic subgroups of CCA patients. (A) The graph shows the integration of *KRAS*-mutant CRISPR/Cas9 *PARP-1* KO clones (dark blue) and respective control clones (light blue) with a previously published dataset of 45 CCA patients with good (pink) and poor (yellow) prognosis. (B) Upper graph shows the integration of *Parp-1*$^{-/-}$ mice (dark blue) and *Parp-1*$^{+/+}$ mice (light blue) with *Kras/Tp53*-induced carcinogenesis with a previously published dataset of 45 CCA patients with good (pink) and poor (yellow) prognosis. Lower graph shows integration of *Parp-1*$^{-/-}$ mice (dark green) and *Parp-1*$^{+/+}$ mice (light green) with *Akt/Nicd* -induced carcinogenesis with a previously published dataset of 45 CCA patients with good (pink) and poor (yellow) prognosis. CCA, cholangiocarcinoma.

information is available as to the role of *PARP-1* expression in the therapeutic response of *KRAS*-mutant iCCA. Here, we demonstrated an upregulation of *PARP-1* expression in *KRAS*-mutant iCCA tissue and cancer-derived cell lines in comparison to normal intrahepatic bile duct tissue and *KRAS*-wildtype cell lines (figure 1). We were able to show that this patient subgroup has significant association with decreased overall and recurrence-free survival (online supplemental figure S1). In concordance with recent studies, a significantly higher expression, and positive correlation of *KRAS* and *PARP-1* in cholangiocarcinoma (CHOL) tumour samples in comparison to normal tissue samples (online supplemental figure S1).[9 30 31]

Our data confirm that knockdown of *PARP-1* by RNAi as well as treatment with Olaparib, an effective PARP-1/2 inhibitor, exerted preferential effects in *KRAS*-mutant cell lines compared with *KRAS*-wildtype cell lines (figure 1, online supplemental figure S2). A comprehensive meta-analysis of Ku *et al* recently confirmed reduced proliferation on PARP inhibition in *KRAS*-mutant MCF10a cells (transfected with mutant *KRAS* constructs) compared with *KRAS*-wildtype. The study also implies that *KRAS*-mutant cells are highly dependent on DDR pathways confirming a synthetic lethality in *KRAS*-mutant cancers, which aligns with our hypothesis for *KRAS*-driven iCCA.[14]

Molecular analyses of iCCA cell lines on *PARP-1* KO confirmed that the lack of PARP-1 results in dysregulation of several DNA repair pathways (BER, DSB repair) predominantly in *KRAS*-mutant iCCA cell lines (figure 1, online supplemental figure S4).[12 14 32] This observation supports the hypothesis that *KRAS*-mutant tumours are more dependent on functioning DDR pathways in general and show preferential impairment of the *PARP-1*-associated DNA repair pathway alt-NHEJ.[13 14] However, stable *PARP-1* depletion lacks the effect of PARP-1-DNA trapping caused by PARP-1 inhibition,[33] which limits therapeutic predictions in this model. Nevertheless, dysregulation of DDR processes on *PARP-1* depletion was explained on the basis of multiple interactions of PARP-1 and PARylation with other DDR factors.[34 35] PARP-1 activation was associated with enhanced activation of the error-prone alt-NHEJ pathway over c-NHEJ by competing with Ku70 protein on the site of DNA damage.[36 37]

In addition to changes in DDR pathways, our transcriptomic data indicate an involvement of apoptotic signalling, inflammatory response and oxidative stress (figure 2, online supplemental figure S4). Further analyses are required to clarify the role of these pathways in the context of tumour initiation and progression and the proposed pro-apoptotic and anti-inflammatory effects of *PARP-1* deficiency and PARPi.[13 32 38] Hähnel *et al* showed that *KRAS*-mutant AML cells are sensitised towards apoptosis on PARP-1 inhibition in combination with the DNA damaging anticancer drug daunorubicin.[13] Further, *PARP-1* deficiency or PARPi was associated with decreased gene expression of proinflammatory cytokines in previous studies.[12 39] Other studies hypothesised that *PARP-1* activity might act as a double-edged sword during carcinogenesis, affecting apoptotic and oxidative processes and proinflammatory signalling, dependent on the cellular metabolic status and state of tumourigenesis.[12 16 23 40 41] Overall, our in vitro experiments exploring diverse modes of PARP-1 inhibition, including RNAi, and CRISPR/Cas9-mediated *PARP-1* KO confirmed that hypersensitivity of *KRAS*-mutant iCCA cell lines is related to altered tumourigenic properties. These findings propose a novel therapeutic strategy for a previously difficult-to-treat subgroup of progressed iCCA patients harbouring *KRAS* mutations. Of note, synergistic effects observed between Olaparib and commonly used chemotherapeutic compounds in *KRAS*-mutant cells indicate that a combination treatment might be of further therapeutic interest and could be pursued in future investigations (online supplemental figure S2D).

To further determine the role of *PARP-1* in tumour initiation and cancer development, we employed a model of *KRAS*-driven cholangiocarcinogenesis in *Parp-1* deficient animals.[11 42–44] In consistence with previous reports, *Parp-1* proficient mice display predominant development of solid iCCA (80%) accompanied by dysplastic hepatocellular foci and nodules as well as early hepatocellular carcinoma in the surrounding liver tissue 10 weeks after HDTV with *Kras*/*Tp53* (figure 3).[11] In stark contrast, in *Parp-1*-deficient mice, *Kras*-induced carcinogenesis was characterised by the absence of cholangiocarcinoma and the presence of multiple dysplastic foci and nodules as well as small HCC with tumourous vein invasion. Importantly, transcriptomic analyses of our in vivo data suggest a pronounced inhibition of NOTCH signalling (figure 4, online supplemental figures S8 and S12), a key oncogenic driver of iCCA and predicted factor for transdifferentiation of hepatocytes towards biliary traits, is present in our PARP-1-deficient lesions.[45 46] Furthermore, Ikenoue *et al* demonstrated that activated *Kras* in combination with active *Pten* results predominantly in HCC, whereas activated *Kras* in combination with homozygous inactive *Pten* leads to iCCA development in vivo.[47] In line with this, *Parp-1* deficiency in our study confirms activation of *Pten*. Taken together, activation or inactivation of the above-mentioned pathways, although not being exclusively specific to cholangiocarcinogenesis, might explain the absence of iCCA and shift towards HCC development in our *Kras*/*Tp53*-induced tumour model under *Parp-1* deficiency. Further studies are clearly warranted to define the underling molecular mechanisms responsible for the phenotypic shift.

Consistent with our in vitro data and previous studies with *Parp-1* deficient mice, our transcriptomic analyses of in vivo data showed enrichment of DNA repair pathways (alt-NHEJ, HR, BER) in all experimental groups of *Parp-1* proficient mice while in *Parp-1*$^{-/-}$ mice DNA repair pathways were not enriched.[32 48] Decreased gene expression of proinflammatory cytokines was already observed in *Parp-1*$^{-/-}$ mice and on PARPi and might explain the predicted inhibition of proinflammatory pathways (NF-κB, TGFβ) in our data (figure 4, online supplemental figures S10 and S12).[12 39] Importantly, neither histopathological assessment nor quantification of tumour burden or molecular analyses revealed a dependency on the *Parp-1* genotype in a non-*Kras*-driven iCCA model (*Akt*/*Nicd*) (figures 3 and 4; online supplemental figures S12 and S13).[45] The results clearly underscore the selective relevance of oncogenic *Kras* in *Parp-1* deficient background. Taken together, our in vivo studies confirm the association of *Parp-1* expression in *Kras*/*Tp53*-driven cholangiocarcinogenesis. Reduced cholangiocarcinoma development under *Parp-1* deficiency could be mechanistically explained by dysregulation of apoptotic and inflammatory processes as well as DDR.

It is well established that *KRAS*-mutated cancers exhibit enhanced replicative stress and constitutively activated stress response pathways.[49] Here, CHK1-mediated cell cycle checkpoints maintain genomic integrity and, thus, CHK1 activation might confer key protective mechanisms that protect *KRAS*-driven cancers from this therapeutic liability. Consistently, we could provide evidence that selective induction of PARP-1 in iCCA could be induced by activation of CHK1 in *KRAS*-mutant iCCA (figure 5). We observed a significant upregulation of *CHK1* in *KRAS*-mutated iCCA cell lines and *Kras*/*Tp53* *Parp-1*$^{+/+}$ mice while inhibiting Parp-1 in Kras/Tp53 Parp-1$^{-/-}$ mice resulted in *Chk1* inhibition, as observed in human patients. Furthermore, *KRAS*-mutated iCCA cells were significantly more

sensitive to CHK1 inhibition by Rabusertib, a selective CHK1 inhibitor, than KRAS-wildtype cells or mouse cells deficient in Parp-1 (figure 5). Inhibition of CHK1 significantly influenced components of HR (online supplemental figure S14). Importantly, inhibition of CHK1 also led to a significant reduction of PARP-1 levels in *KRAS*-mutant. When rabusertib was combined with Olaparib, there was no induction of synergistic effects, further implying a potential regulatory role of CHK1 (figure 5). These investigations are in line with several other recent investigations that established a formal association between CHK1 and PARP-1 in highly replicative cancers that rely on a functional DDR, particularly one mediated by HR.[50 51] Studies have also described a direct interaction between CHK1 and PARP-1 at the DNA damage site and subsequent promotion of HR.[52]

Thus, we propose a regulatory axis involving CHK1-mediated PARP-1 activation induced by replicative stress in *KRAS*-mutant iCCA that maintains cellular survival in this subtype of iCCA.

To validate our findings in authentic human tumours, we integrated our in vitro and in vivo findings with a publicly available dataset of well-characterised CCA patients.[8] Consistently, transcriptome profiles of the *PARP-1*-deficient cell lines as well as control cell lines with different established prognostic subgroups of PLC (poor and good prognosis) revealed a shift of *KRAS*-mutant iCCA cell lines from poor to good prognosis on *PARP-1* KO (figure 6). In concordance, *Parp-1* deficient samples from mice injected with *Kras/Tp53* clustered with good prognosis iCCA patient samples, whereas *Parp-1* proficient samples grouped with poor prognosis. Interestingly, this prognostic shift was not visible in *Akt/Nicd*-induced tumour samples, which clustered randomly together with poor prognostic patients. Hence, the obtained data clearly confirm a clear synthetic vulnerability and provide a rational for therapeutic targeting of PARP-1 in *KRAS*-mutant iCCA patients.

CONCLUSION

In conclusion, the study presented confirms upregulation of *PARP-1* and hypersensitivity towards PARP-1-based intervention preferentially detectable in *KRAS*-mutant iCCA in vitro and in vivo. Mechanistically, our data revealed that *PARP-1* inhibition provoked downregulation of DSB repair pathways and inhibition of oxidative and inflammatory processes.[13] Thus, our data open novel therapeutic options for this difficult-to-treat iCCA subgroup that warrant further clinical investigations (online supplemental visual abstract).

Author affiliations
[1]First Department of Internal Medicine, University Medical Center of the Johannes Gutenberg University, Mainz, Germany
[2]Department of Medicine I, University Medical Center Schleswig Holstein Campus Lübeck, Lübeck, Germany
[3]Institute of Pathology, University Medical Center of the Johannes Gutenberg University, Mainz, Germany
[4]Tissue Biobank of the University Medical Center of the Johannes Gutenberg University, Mainz, Germany
[5]Cardiology Angiology, University Medical Centre, Mannheim, Germany
[6]Department of Hematology, Medical Oncology and Pneumology, University Medical Center of the Johannes Gutenberg University, Mainz, Germany
[7]Department of Chemistry, RPTU Kaiserslautern-Landau, Kaiserslautern, Germany
[8]Department of Health and Medical Sciences, University of Copenhagen Biotech Research & Innovation Centre, Kobenhavn, Denmark
[9]Department of Internal Medicine II, Klinikum rechts der Isar der Technischen Universitat, München, Germany
[10]Department of Gastroenterology, Hepatology, and Endocrinology, Hannover Medical School, Hannover, Germany
[11]Laboratory of Human Carcinogenesis, National Cancer Institute, Center for Cancer Research, Bethesda, Maryland, USA
[12]Liver Cancer Program, Center for Cancer Research, National Cancer Institute, Bethesda, Maryland, USA
[13]Institute of Pathology, University Medical Centre Mannheim, University of Heidelberg, Mannheim, Germany
[14]Institute of Pathology, University Hospital Basel, Basel, Switzerland
[15]Institute of Nutritional Medicine, University Medical Center Schleswig Holstein Campus Lübeck, Lübeck, Germany
[16]Department of Systems Biology, The University of Texas MD Anderson Cancer Center, Houston, Texas, USA
[17]Institute of Pathology, University Hospital Heidelberg, Heidelberg, Germany
[18]Department of Toxicology, University Medical Center of the Johannes Gutenberg University, Mainz, Germany

X Jesper B Andersen @jaboeje

Acknowledgements JUM and FLK thank Monika Herr for excellent technical support. Sorting of CRISPR/Cas9 clones was performed with the support of the Core Facility Flow Cytometry (CFFC) of the PaulKlein Center for Immune Intervention (PZKI), University Medical Center, Mainz. Tissue staining were provided by the tissue bank of the University Medical Center, Mainz in accordance with the regulations of the tissue biobank and the approval of the ethics committee of University Medical Center, Mainz. Aspects of this article are part of the doctoral thesis of FLK.

Contributors Conceptualisation: JUM and FLK; Data curation: FLK, DC, DB, SS, JC, CZ, BKS, TG, CJO'R, CS, SD, UE, AS, LM, XWW, SR, JBA, PRG and JUM; Resources: PH, TK, JF, UE, TG, MSM and BK; Formal analysis: JUM, FLK, DC, DB and BKS; Writing: JUM, FLK and DC. Guarantor: JUM; All authors discussed the results and critically commented on the manuscript.

Funding JUM is supported by grants from the Wilhelm Sander Foundation (2021.089.1) and the Volkswagen Foundation (Lichtenberg program). SR was supported by Deutsche Forschungsgemeinschaft (DFG, Project-ID 314905040) within SFB/TRR 209 Liver Cancer, by Eurostars (grant E! 113707, LiverQR) and by the German Cancer Aid (no. 70113922). XWW is supported by grants (ZIA BC010313 and ZIA BC011870) from the Intramural Research Program of the Center for Cancer Research of the National Cancer Institute.

Competing interests None declared.

Patient and public involvement Patients and/or the public were not involved in the design, or conduct, or reporting, or dissemination plans of this research.

Patient consent for publication Not applicable.

Provenance and peer review Not commissioned; externally peer reviewed.

Data availability statement All data relevant to the study are included in the article or uploaded as online supplemental information.

ORCID iDs
Timo Gaiser http://orcid.org/0000-0002-6022-073X
Stefanie Derer http://orcid.org/0000-0002-6142-5577
Ju-Seog Lee http://orcid.org/0000-0002-5666-9753
Stephanie Roessler http://orcid.org/0000-0002-5333-5942
Jesper B Andersen http://orcid.org/0000-0003-1760-5244
Jens U Marquardt http://orcid.org/0000-0002-8314-2682

REFERENCES

1 Khan SA, Tavolari S, Brandi G. Cholangiocarcinoma: epidemiology and risk factors. *Liver International* 2019;39:19–31.
2 Banales JM, Marin JJG, Lamarca A, *et al*. Cholangiocarcinoma 2020: the next horizon in mechanisms and management. *Nat Rev Gastroenterol Hepatol* 2020;17:557–88.
3 Clements O, Eliahoo J, Kim JU, *et al*. Risk factors for Intrahepatic and extrahepatic Cholangiocarcinoma: a systematic review and meta-analysis. *J Hepatol* 2020;72:95–103.

4 Braconi C, Roessler S, Kruk B, *et al*. Molecular perturbations in Cholangiocarcinoma: is it time for precision medicine *Liver International* 2019;39:32–42.
5 Czauderna C, Kirstein MM, Tews HC, *et al*. Molecular subtypes and precision oncology in Intrahepatic Cholangiocarcinoma. *J Clin Med* 2021;10:2803.
6 Moeini A, Sia D, Bardeesy N, *et al*. Molecular pathogenesis and targeted therapies for Intrahepatic Cholangiocarcinoma. *Clinical Cancer Research* 2016;22:291–300.
7 Andersen JB. Molecular pathogenesis of Intrahepatic Cholangiocarcinoma. *J Hepato Biliary Pancreat* 2015;22:101–13.
8 Andersen JB, Spee B, Blechacz BR, *et al*. Genomic and genetic characterization of Cholangiocarcinoma identifies therapeutic targets for tyrosine kinase inhibitors. *Gastroenterology* 2012;142:1021–31.
9 Marquardt JU, Andersen JB, Thorgeirsson SS. Functional and genetic deconstruction of the cellular origin in liver cancer. *Nat Rev Cancer* 2015;15:653–67.
10 Grabocka E, Commisso C, Bar-Sagi D. Molecular pathways: targeting the dependence of mutant RAS cancers on the DNA damage response. *Clin Cancer Res* 2015;21:1243–7.
11 O'Dell MR, Huang JL, Whitney-Miller CL, *et al*. Kras(G12D) and P53 Mutation cause primary Intrahepatic Cholangiocarcinoma. *Cancer Res* 2012;72:1557–67.
12 Dörsam B, Seiwert N, Foersch S, *et al*. PARP-1 protects against colorectal tumor induction, but promotes inflammation-driven colorectal tumor progression. *Proc Natl Acad Sci U S A* 2018;115:E4061–70.
13 Hähnel PS, Enders B, Sasca D, *et al*. Targeting components of the alternative NHEJ pathway sensitizes KRAS mutant Leukemic cells to chemotherapy. *Blood* 2014;123:2355–66.
14 Ku AA, Hu H-M, Zhao X, *et al*. Integration of multiple biological contexts reveals principles of synthetic lethality that affect reproducibility. *Nat Commun* 2020;11:2375.
15 Pascal JM, Ellenberger T. The rise and fall of Poly(ADP-ribose): an enzymatic perspective. *DNA Repair* 2015;32:10–6.
16 Ray Chaudhuri A, Nussenzweig A. The Multifaceted roles of Parp1 in DNA repair and chromatin remodelling. *Nat Rev Mol Cell Biol* 2017;18:610–21.
17 Lord CJ, Ashworth A. PARP inhibitors: synthetic lethality in the clinic. *Science* 2017;355:1152–8.
18 Kaufman B, Shapira-Frommer R, Schmutzler RK, *et al*. Olaparib monotherapy in patients with advanced cancer and a Germline Brca1/2 Mutation. *J Clin Oncol* 2015;33:244–50.
19 Jain PG, Patel BD. Medicinal chemistry approaches of poly ADP-ribose polymerase 1 (Parp1) inhibitors as anticancer agents - A recent update. *Eur J Med Chem* 2019;165:198–215.
20 Ricci AD, Rizzo A, Bonucci C, *et al*. PARP inhibitors in biliary tract cancer: A new kid on the block *Medicines* 2020;7:54.
21 Tang Z, Kang B, Li C, *et al*. Gepia2: an enhanced web server for large-scale expression profiling and interactive analysis. *Nucleic Acids Res* 2019;47:W556–60.
22 Weinstein JN, Collisson EA, Mills GB, *et al*. The cancer genome Atlas Pan-cancer analysis project. *Nat Genet* 2013;45:1113–20.
23 Pazzaglia S, Pioli C. Multifaceted role of PARP-1 in DNA repair and inflammation: pathological and therapeutic implications in cancer and non-cancer diseases. *Cells* 2019;9:41.
24 Bi F-F, Li D, Yang Q. Hypomethylation of ETS transcription factor binding sites and upregulation of Parp1 expression in endometrial cancer. *Biomed Res Int* 2013;2013:946268.
25 Byers LA, Wang J, Nilsson MB, *et al*. Proteomic profiling identifies Dysregulated pathways in small cell lung cancer and novel therapeutic targets including Parp1. *Cancer Discov* 2012;2:798–811.
26 Dziaman T, Ludwiczak H, Ciesla JM, *et al*. PARP-1 expression is increased in colon adenoma and carcinoma and correlates with Ogg1. *PLoS One* 2014;9:e115558.
27 Liu Y, Zhang Y, Zhao Y, *et al*. High PARP-1 expression is associated with tumor invasion and poor prognosis in gastric cancer. *Oncol Lett* 2016;12:3825–35.
28 Xu F, Sun Y, Yang S-Z, *et al*. Cytoplasmic PARP-1 promotes Pancreatic cancer tumorigenesis and resistance. *Int J Cancer* 2019;145:474–83.
29 Fahrer J, Kaina B. O6-Methylguanine-DNA methyltransferase in the defense against N-nitroso compounds and colorectal cancer. *Carcinogenesis* 2013;34:2435–42.
30 Taketomi A, Shirabe K, Muto J, *et al*. A rare point Mutation in the Ras Oncogene in hepatocellular carcinoma. *Surg Today* 2013;43:289–92.
31 Xue R, Chen L, Zhang C, *et al*. Genomic and Transcriptomic profiling of combined hepatocellular and Intrahepatic Cholangiocarcinoma reveals distinct molecular subtypes. *Cancer Cell* 2019;35:932–47.
32 de Murcia JM, Niedergang C, Trucco C, *et al*. Requirement of Poly(ADP-ribose) polymerase in recovery from DNA damage in mice and in cells. *Proc Natl Acad Sci U S A* 1997;94:7303–7.
33 Murai J, Huang SN, Das BB, *et al*. Trapping of Parp1 and Parp2 by clinical PARP inhibitors. *Cancer Res* 2012;72:5588–99.
34 Isabelle M, Moreel X, Gagné J-P, *et al*. Investigation of PARP-1, PARP-2, and PARG Interactomes by affinity-purification mass Spectrometry. *Proteome Sci* 2010;8:22.
35 Pines A, Vrouwe MG, Marteijn JA, *et al*. Parp1 promotes nucleotide Excision repair through Ddb2 Stabilization and recruitment of Alc1. *J Cell Biol* 2012;199:235–49.
36 Paddock MN, Bauman AT, Higdon R, *et al*. Competition between PARP-1 and Ku70 control the decision between high-fidelity and Mutagenic DNA repair. *DNA Repair (Amst)* 2011;10:338–43.
37 Wang M, Wu W, Wu W, *et al*. PARP-1 and Ku compete for repair of DNA double strand breaks by distinct NHEJ pathways. *Nucleic Acids Res* 2006;34:6170–82.
38 Zhong L, Wang R, Wang Y, *et al*. Dual inhibition of VEGF and PARP suppresses KRAS-mutant colorectal cancer. *Neoplasia* 2020;22:365–75.
39 Quiles-Perez R, Muñoz-Gámez JA, Ruiz-Extremera Á, *et al*. Inhibition of poly adenosine diphosphate-ribose polymerase decreases hepatocellular carcinoma growth by modulation of tumor-related gene expression. *Hepatology* 2010;51:255–66.
40 Morales J, Li L, Fattah FJ, *et al*. Review of poly (ADP-ribose) polymerase (PARP) mechanisms of action and rationale for targeting in cancer and other diseases. *Crit Rev Eukaryot Gene Expr* 2014;24:15–28.
41 Swindall AF, Stanley JA, Yang ES. PARP-1: friend or foe of DNA damage and repair in tumorigenesis *Cancers (Basel)* 2013;5:943–58.
42 Gürlevik E, Fleischmann-Mundt B, Armbrecht N, *et al*. Adjuvant Gemcitabine therapy improves survival in a locally induced, R0-Resectable model of metastatic Intrahepatic Cholangiocarcinoma. *Hepatology* 2013;58:1031–41.
43 Hill MA, Alexander WB, Guo B, *et al*. Kras and Tp53 mutations cause Cholangiocyte- and hepatocyte-derived Cholangiocarcinoma. *Cancer Res* 2018;78:4445–51.
44 Saborowski A, Lehmann U, Vogel A. FGFR inhibitors in Cholangiocarcinoma: what's now and what's next. *Ther Adv Med Oncol* 2020;12.
45 Fan B, Malato Y, Calvisi DF, *et al*. Cholangiocarcinomas can originate from hepatocytes in mice. *J Clin Invest* 2012;122:63212:2911–5:.
46 Zender S, Nickeleit I, Wuestefeld T, *et al*. A critical role for notch signaling in the formation of Cholangiocellular Carcinomas. *Cancer Cell* 2016;30:353–6.
47 Ikenoue T, Terakado Y, Nakagawa H, *et al*. A novel mouse model of Intrahepatic Cholangiocarcinoma induced by liver-specific Kras activation and Pten deletion. *Sci Rep* 2016;6:23899.
48 Wang ZQ, Auer B, Stingl L, *et al*. Mice lacking ADPRT and Poly(ADP-Ribosyl)Ation develop normally but are susceptible to skin disease. *Genes Dev* 1995;9:509–20.
49 Al Zubaidi T, Gehrisch OHF, Genois M-M, *et al*. Targeting the DNA replication stress phenotype of KRAS mutant cancer cells. *Sci Rep* 2021;11:3656.
50 Smith HL, Prendergast L, Curtin NJ. Exploring the synergy between PARP and Chk1 inhibition in matched Brca2 mutant and corrected cells. *Cancers (Basel)* 2020;12:878.
51 Vance S, Liu E, Zhao L, *et al*. Selective Radiosensitization of P53 mutant Pancreatic cancer cells by combined inhibition of Chk1 and Parp1. *Cell Cycle* 2011;10:4321–9.
52 Peng B, Shi R, Bian J, *et al*. Parp1 and Chk1 coordinate Plk1 enzymatic activity during the DNA damage response to promote Homologous Recombination-mediated repair. *Nucleic Acids Res* 2021;49:7554–70.